ELSEVIER

Earth and Planetary Science Letters 184 (2000) 181–197

EPSL

www.elsevier.com/locate/epsl

Modelling the emplacement of compound lava flows

S. Blake *, B.C. Bruno [1]

Department of Earth Sciences, The Open University, Milton Keynes MK7 6AA, UK

Received 5 May 2000; received in revised form 12 September 2000; accepted 19 September 2000

Abstract

The physical variables controlling crust-dominated lava flow have been investigated using laboratory experiments in which molten polyglycol wax was extruded from a point source on to a horizontal plane under cold water. The wax initially spread axisymmetrically and a crust of solid wax grew. Eventually wax broke out from the flow's periphery, sending out a flow lobe which in turn cooled and produced another breakout. The process repeated itself many times, building a 'compound lava'. The time for the first breakout to form correlates well with the theoretically predicted time (t_c) required for cooling to form a crust thick enough for its strength to limit the flow's spreading rate. This time is proportional to the product of effusion rate (Q) and initial magma viscosity (μ) and inversely proportional to the square of the crust strength at the flow front. The number of flow units and the apparent fractal dimension of the flow perimeter increase with time normalised by t_c. Our model illuminates the physical basis for the observation by Walker [G.P.L. Walker, Bull. Volcanol. 35 (1972) 579–590] that compound lava flows form by slow effusion of low viscosity magma, whereas faster effusion and higher viscosity favour lavas with fewer flow units. Because compound flows require $t \gg t_c$, and given that $t_c \propto Q\mu$ and the relationship between volume and effusion rate is $V = Qt$, simple and compound lava flows are predicted to fall in separate fields on a graph of μ against V/Q^2, all else being equal. Compound flows plot at small values of μ and large values of V/Q^2, with the position of the simple/compound boundary defined by field data implying a crust strength of order 10^4 Pa for basaltic to intermediate lavas. Whether a flow remains as a simple flow or matures into a compound flow field depends on the combined effect of viscosity, eruption rate and eruption duration (and hence volume) and these parameters need to be taken in to account when using morphology to infer eruption conditions. In particular, compound flows form from terrestrial subaerial point source eruptions on horizontal ground when $\mu < 0.002V/Q^2$.

Keywords: lava; emplacement; eruptions; models; laboratory studies

1. Introduction

Some lava flows consist of a single stream of lava extending directly from the vent to the flow front. Such lavas are termed simple flows [1]. In the contrasting case of compound flows, the lava may comprise a few lobes or countless smaller branches that have budded from the main stream and each other. In this paper we model the con-

* Corresponding author. Tel.: +44-1908-652889; Fax: +44-1908-655151; E-mail: s.blake@open.ac.uk

[1] Present address: Natural Sciences Building 14, Broward Community College, 3501 S.W. Davie Road, Davie, FL 33314, USA.

0012-821X/00/$ – see front matter
PII: S0012-821X(00)00278-8

tinuum of flow types but pay most attention to the conditions under which breakouts and compound lavas form. Such insights are necessary in order to predict the likely flow behaviour of any lava in the future and to interpret the effusion conditions or magma properties of ancient flows, such as flood basalts and extraterrestrial lavas, from their observed features.

Importantly, field observations of flowing lavas have shown that their progress and morphology are strongly influenced by the growth, deformation and rupture of their cool skin or crust [2–5]. The role of the crust is also clear from analogue experiments using wax that have shown how solidification leads to flow channelisation, the formation of breakouts and flow lobes, and the development of various surface textures [6–12]. In particular, Fink and Griffiths [7,8,12–15] related surface morphology to the time required for the surface of a flowing lava to reach its solidification temperature. In this paper we use theoretical and laboratory models to investigate the parameters controlling the growth rate of crust and the onset of breakouts. Our study differs from those of Fink and Griffiths in that we concentrate on the time scale for breakouts to form, the long-term evolution of flow fields and the apparent fractal dimension of lava flow margins. We compare our model with geological data and highlight the importance of eruption duration, viscosity and effusion rate on flow morphology.

2. Transition to crust-controlled spreading

In general, the progress and morphology of a lava flow are limited by the rheology of the hot lava and the rheology of the cold skin or crust that grows over it. Here we concentrate on flows that have negligible yield strength when erupted but which grow a cool surface crust that possesses a mechanical strength. The flow of the lava is initially governed by the viscosity of the hot erupted magma, μ, but after some critical cooling time the rheology of the lava crust becomes dominant and the flow behaviour enters a new regime. To investigate this flow transition we consider the effusion of lava from a point source onto a flat horizontal surface. The lava is denser than its environment by $\Delta\rho$, and produces an axisymmetric flow with radius $R(t)$ and height $H(t)$. Its volume is taken to increase as:

$$V = Qt^{\alpha} \tag{1}$$

where α is a constant and Q has dimensions of $(\text{length})^3(\text{time})^{-\alpha}$; when $\alpha = 1$, the effusion rate is Q and has a constant value.

Following Griffiths and Fink [16], initial spreading is governed by a balance between the buoyancy force driving spreading [16]:

$$F_B \sim g\Delta\rho H^2 R \tag{2}$$

and the resistive viscous force acting over the flow base:

$$F_\mu \sim \frac{\mu R^3}{Ht} \tag{3}$$

which, using Eq. 1, gives the spreading laws [16,17]:

$$R \sim \left(\frac{g\Delta\rho Q^3}{\mu}\right)^{1/8} t^{(3\alpha+1)/8} \tag{4}$$

$$H \sim \left(\frac{\mu Q}{g\Delta\rho}\right)^{1/4} t^{(\alpha-1)/4} \tag{5}$$

Cooling of the lava's surface causes a thermal and hence rheological boundary layer of thickness δ to grow by conduction, thickening with the square root of time:

$$\delta = s\sqrt{\kappa t} \tag{6}$$

where s is a constant of order 1 whose value depends on the details of the thermal exchange between the lava and its environment and the thermal boundary conditions and κ is the lava's thermal diffusivity [14,15,18,19]. The dependence of crust thickness on $\sqrt{t}$ has been measured on active lavas [2].

The resistive force due to the strength σ of cold crust at the flow front is [16]:

$$F_\sigma \sim \sigma R\delta \tag{7}$$

It follows that the ratio of the forces due to crust strength and interior viscosity changes according to:

$$\frac{F_\sigma}{F_\mu} \sim \left(\frac{\sigma^2 s^2 \kappa}{g\Delta\rho\,\mu\,Q}\right)^{1/2} t^{(1-\alpha/2)} \quad (8)$$

Thus, for $\alpha < 2$ the strength of the crust becomes more important with time, and the transition to crust control is achieved after:

$$t_{\mathrm{crust}} \sim \left(\frac{g\Delta\rho\,\mu\,Q}{\sigma^2 s^2 \kappa}\right)^{1/(2-\alpha)} \quad (9)$$

Following the analogous argument for flow from a line source (fissure) with volume erupted per unit length of source $v \sim qt^\alpha$ yields (for $\alpha < 9/8$):

$$t_{\mathrm{crust}} \sim \left(\frac{(\mu^2 (g\Delta\rho)^3 q^4)^{1/5}}{\sigma s \kappa^{1/2}}\right)^{10/(9-8\alpha)} \quad (10)$$

Eqs. 9 and 10 (with $s = 1$) are the correct versions of Eqs. 11 and 12 of Griffiths and Fink [16] which were wrongly printed in their paper (Griffiths, 1998, personal communication). In what follows we consider the case of constant effusion rate ($\alpha = 1$) from a point source, for which Eq. 9 becomes:

$$t_{\mathrm{crust}} \sim \frac{g\Delta\rho\,\mu\,Q}{\sigma^2 s^2 \kappa} \quad (11)$$

Once t_{crust} has been reached, two possible behaviours can be envisaged. The first is that axisymmetric flow continues but at a rate determined by the strength of the thickening crust rather than the viscosity of the hot interior. Thus, for constant effusion rate, Griffiths and Fink [16] predict a change from spreading described by $R \sim (g\Delta\rho Q^3/\mu)^{1/8} t^{1/2}$ (see Eq. 4) to spreading described by:

$$R \sim \left(\frac{g\Delta\rho\,Q^2}{\sigma s \kappa^{1/2}}\right)^{1/4} t^{3/8} \quad (12)$$

The second possibility is that on entering the regime limited by crust strength, deformation of the crust is focused on isolated weak spots, allowing breakouts of hot fluid lava to escape from ruptures in the retaining crust. Here, t_{crust} represents the time at which the pattern of spreading changes from even radial spreading to the spatially irregular development of breakouts and flow lobes. This type of behaviour characterises analogue laboratory experiments [7,8,16] and the budding of pillows, tubes, pahoehoe toes and other breakouts in many lava flows [2,20].

As already noted, the exact rate at which the crust thickens depends on the thermal boundary conditions and heat transfer mechanisms at the surface and in the lava. Thus, the coefficient s in Eq. 6 is a function of the dimensionless temperature of the isotherm defining the edge of the rheological crust:

$$\theta_{\mathrm{s}} = \frac{T_{\mathrm{solid}} - T_{\mathrm{a}}}{T_{\mathrm{m}} - T_{\mathrm{a}}} \quad (13)$$

and the Stefan number

$$St = \frac{L}{c(T_{\mathrm{m}} - T_{\mathrm{solid}})} \quad (14)$$

where T_{solid} is the solidification temperature of the crust, T_{a} is the ambient temperature, T_{m} is the effusion temperature of the magma, L is the latent heat of solidification and c is the specific heat capacity of the magma [18,21]. In addition, the outward movement of the spreading lava can advect cool surface material to the flow front (as seen by Stasiuk et al. [22] in experiments with liquid syrup) increasing the rate at which the crust at the flow front thickens. The importance of this effect will increase with increasing Peclet number, defined as the ratio of the time scale required to conduct heat through the flow depth to that required to advect heat radially by a distance H [7]:

$$Pe = \left(\frac{Q^3 g\Delta\rho}{\mu}\right)^{1/4} \frac{1}{\kappa} \quad (15)$$

Lastly, s will also be influenced by the surface heat flux (F) due to conduction, free convection, forced convection or radiation from the surface. The dimensionless heat flux, or Nusselt number, is:

$$Nu = \frac{HF}{\kappa\rho c(T_{\mathrm{m}} - T_{\mathrm{a}})} \quad (16)$$

The separate influences of θ_s, *St*, *Pe* and *Nu* are compounded in the value of s in t_{crust} (Eq. 11). The transition time scale can also be considered to be described by the simplified time scale:

$$t_c = \frac{\mu g \Delta \rho Q}{\sigma^2 \kappa} \quad (17)$$

together with θ_s, *St*, *Pe* and *Nu*.

3. Experimental method

We conducted experiments with pharmaceutical grade polyethylene glycol 600 wax (PEG) to simulate lava flow emplacement, following the methods of Fink and Griffiths [7]. The solidification temperature of our batch of wax was $T_{solid} = 19.6$°C. The viscosity (in Pa s) of PEG was measured between 22 and 52°C by rotational viscometry:

$$\mu = 1.262 \times 10^{-4} T^2 - 0.01340 T + 0.4017 \quad (18)$$

Other properties of PEG are $\kappa = 8.6 \times 10^{-8}$ m^2 s^{-1} [12], $c = 2.5 \times 10^3$ J kg^{-1} °C^{-1} (manufacturer's figure), $L = 1.46 \times 10^5$ J kg^{-1} (manufacturer's figure), strength of solid PEG $\sigma = 40 \pm 20$ Pa [16] (but see Section 5.3), density (kg m^{-3}) as a function of temperature [8]:

$$\rho = 1147.1 - 1.04 T \quad (19)$$

About 1, 1.5 or 2 l of liquid PEG was 'erupted' through a 1 cm diameter hole centrally located in the base of a perspex tank measuring 0.90×0.90 m (internal dimensions) and filled to a depth of ca. 0.25 m with cold water. Before each run the base of the tank was set horizontal using a spirit level. A constant effusion rate was maintained using a peristaltic pump. The wax contained a few drops of food colouring to help visualise the transition from transparent liquid to opaque solid. The initial wax temperature (T_m) was varied between 27.7 and 48.2°C. The water temperature (T_a) was varied between 5.9 and 11.5°C such that $0.28 \leq \theta_s \leq 0.63$ and $2.0 \leq St \leq 7.2$. In most cases, we repeated each set of experimental conditions (Table 1).

4. Description of the experimental flows

All experiments started with hot wax flowing radially away from the source. After 1–16 s, solid crust appeared on the surface of the spreading wax, or around its edge. The wax continued to spread, but with an uneven outline. In all of the experiments except those with the fastest effusion rates, the solid crust either ruptured or was overridden by liquid wax emerging from the vent behind the frozen flow margin. In both cases, a new lobe of liquid wax budded from the original flow after 16–100 s and in turn partly crusted over and spawned a further breakout. Eventually a complex field of many overlapping flow lobes or pillows, analogous to a compound lava field, was established (Fig. 1).

Breakouts formed more frequently for lower effusion rates and higher values of θ_s, as reported previously [6,7,8,10]. At low effusion rate and high θ_s, the emerging wax crusted over almost immediately (e.g. experiment CS1 illustrated in Fig. 1a and with conditions given in Table 1) and successive breakouts from the flow margin and surface built a pile of small lobes or pillows (Fig. 1b). Places where liquid wax is flowing over the surface from boccas in the solid wax surface, presumably fed by an arterial system of tubes within the wax, show up as darker regions. During the course of the experiment different surface boccas became established and then shut down.

At a higher flow rate (e.g. experiment VCT1)

→

Fig. 1. Illustrations of early and late morphologies in four experiments covering different values of θ_s and Q. (a) CS1, $\theta_s = 0.522$, $Q = 6.9 \times 10^{-7}$ m^3 s^{-1} after time $t = 25$ s; (b) CS1 at $t = 1\,884$ s; (c) VCT1, $\theta_s = 0.554$, $Q = 3.37 \times 10^{-6}$ m^3 s^{-1} at $t = 24$ s; (d) VCT1 at $t = 385$ s; (e) PSH1, $\theta_s = 0.340$, $Q = 7 \times 10^{-7}$ m^3 s^{-1} at $t = 28$ s; (f) PSH1 at $t = 1\,857$ s; (g) PR3, $\theta_s = 0.351$, $Q = 3.5 \times 10^{-6}$ m^3 s^{-1} at $t = 25$ s; (h) PR3 at $t = 371$ s. (b), (d), (f) and (h) show flows after 1.3 l of PEG have been effused. Concentric circles are 0.8 cm apart; heavy concentric circles are 4 cm apart.

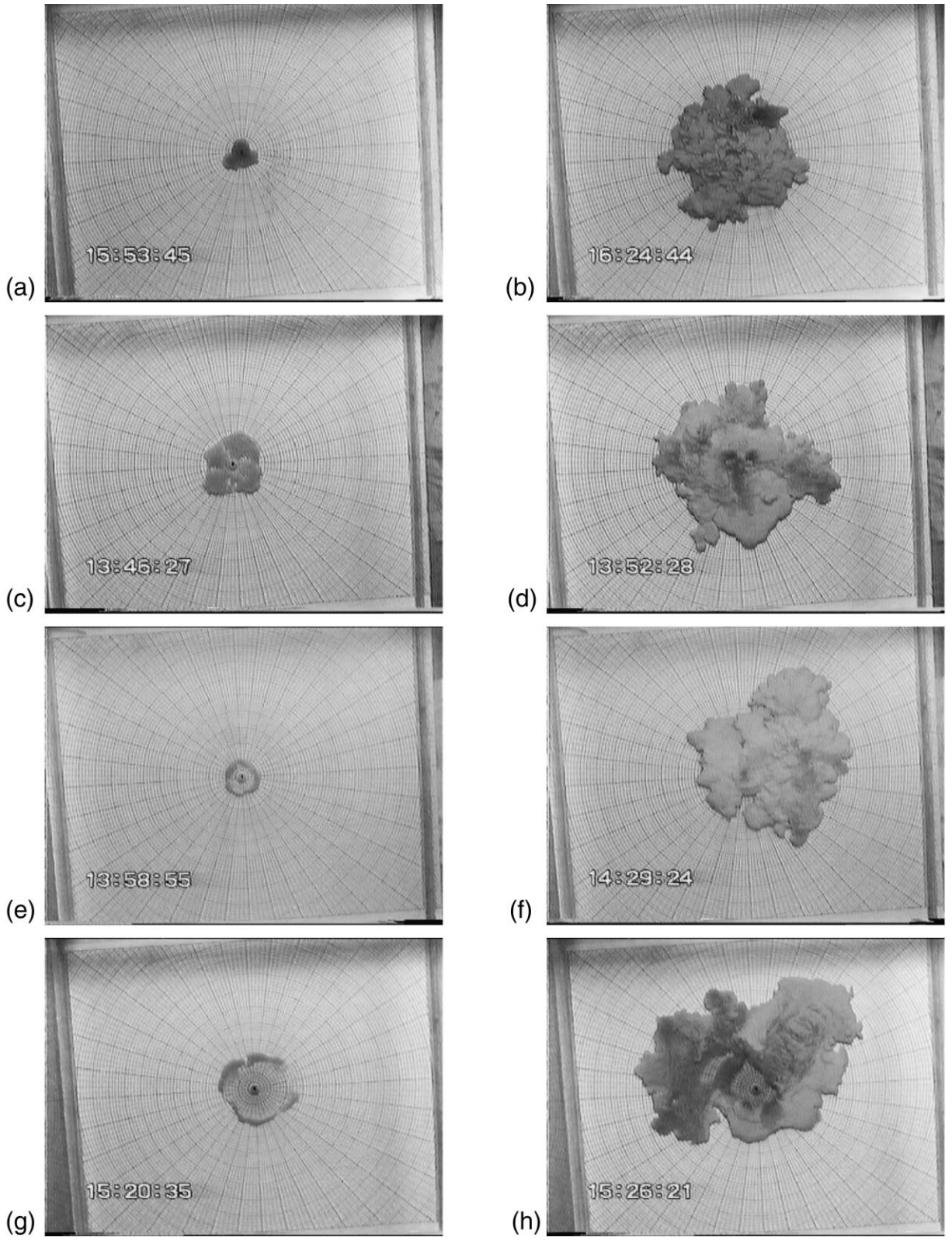
(a)
15:53:45
(b)
16:24:44
(c)
13:46:27
(d)
13:52:28
(e)
13:58:55
(f)
14:29:24
(g)
15:20:35
(h)
15:26:21

Table 1
Summary of experimental data and results

Experiment	Q	T_{water}	T_{wax}	Duration	Final volume	θ_s	St	Pe	Nu	t_s	t_{b1}	D
	($cm^3\ s^{-1}$)	(°C)	(°C)	(s)	(l)			($\times 10^{-3}$)		(s)	(s)	
G1	1.50	11.5	39	1090	1.635	0.295	3.01	5.53	4.20		102	1.120
G2	1.50	8.6	39	975	1.463	0.362	3.01	5.53	4.23	3	28	1.090
G3	1.50	8.8	39	1265	1.898	0.358	3.01	5.53	4.23	6	53	1.130
G4	1.50	9.4	39	1151	1.727	0.345	3.01	5.53	4.22	5	62	1.150
G5	1.50	9.5	39	982	1.473	0.342	3.01	5.53	4.22	8	53	
GR1	1.50	9.2	38.3	887	1.331	0.357	3.12	5.49	4.22	5	47	1.144
GR2	1.50	9.2	38.9	930	1.395	0.350	3.03	5.52	4.22	7	54	1.155
GR3	1.50	9.2	38	932	1.398	0.361	3.17	5.47	4.22	7	47	1.119
PP1	3.50	9.2	38.7	550	1.925	0.353	3.06	10.4	5.22	9	43	
PP2	3.50	9.4	38.8	560	1.960	0.347	3.04	10.4	5.22	6	54	
PP3	3.50	10	39.5	531	1.859	0.325	2.93	10.4	5.22	6	41	
PP4	3.50	9.4	39.5	550	1.925	0.339	2.93	10.4	5.22	7	66	
PP5	3.50	9.3	39.5	535	1.873	0.341	2.93	10.4	5.22	6	63	
PR1	3.50	9.3	39.2	385	1.348	0.344	2.98	10.4	5.22	6	50	1.086
PR2	3.50	9.0	39	377	1.320	0.353	3.01	10.4	5.22	6	75	1.097
PR3	3.50	9.1	39	390	1.365	0.351	3.01	10.5	5.22	8	58	1.142
PR4	3.50	9.0	39	377	1.320	0.353	3.01	10.5	5.22	5	48	1.133
PR5	3.50	9.3	38.8	361	1.264	0.349	3.04	10.5	5.22	4	95	1.122
P4	1.50	6.9	36.3	510	0.765	0.432	3.50	5.37	4.22			1.091
P5	1.50	6.7	36	634	0.951	0.440	3.56	5.36	4.22			1.148
P6	1.50	7.1	37.8	490	0.735	0.407	3.21	5.46	4.23	6	36	1.102
P7	1.50	7.0	35.6	570	0.855	0.441	3.65	5.33	4.22	1	46	1.134
Y3	9.40	7.3	37.9	85	0.799	0.402	3.19	21.6	6.69	4		1.057
Y4	9.40	7.5	37.5	95	0.893	0.403	3.26	21.6	6.69	1		1.052
Y5	9.40	7.5	37.8	95	0.893	0.399	3.21	21.6	6.69	6		1.070
Y6	9.40	7.6	37.5	96	0.902	0.401	3.26	21.5	6.69	3		1.058
Y7	9.40	7.5	37.8	95	0.893	0.399	3.21	2.16	6.69	2		1.066
B1	17.0	7.6	37.1	66	1.122	0.407	3.34	33.5	7.75			1.061
B2	17.0	7.3	37.2	54	0.918	0.411	3.32	33.5	7.75	2		1.049
B3	17.0	7.1	36.8	75	1.275	0.421	3.40	33.4	7.75	2		1.061
B4	17.0	7.5	37.4	67	1.139	0.405	3.28	33.6	7.75	3		1.049
B5	17.0	7.5	37.7	66	1.122	0.401	3.23	33.7	7.76	3		1.049
B6	17.0	7.5	37.7	61	1.037	0.401	3.23	33.7	7.76	4		1.052
B7	17.0	7.4	38	62	1.054	0.399	3.17	33.8	7.76	2		1.049
PD1	1.50	6.4	29.9	1162	1.743	0.562	5.67	5.02	4.16	3	38	
PD2	3.50	6.0	30.6	515	1.803	0.553	5.31	9.54	5.16	2	33	
PD3	9.40	6.1	30.8	196	1.842	0.547	5.21	20.1	6.61	2	41	
PD4	1.50	6.3	42.9	1120	1.680	0.363	2.51	5.73	4.26	3	29	
PDR1	1.55	6.5	30.5	825	1.279	0.546	5.36	5.17	4.20	4	34	1.160
PDR2	3.40	6.3	31.2	385	1.309	0.534	5.03	9.40	5.13	1	47	1.139
PDR3	9.10	6.1	31	141	1.283	0.542	5.12	19.6	6.56	1	57	1.080
PDR6	9.70	9.0	39	141	1.368	0.353	3.01	22.4	6.74	7	33	1.076
VCS1	0.76	6.3	29.8	1996	1.517	0.566	5.73	3.01	3.51	4	27	1.188
VCS2	0.76	5.9	27.7	1986	1.509	0.628	7.21	2.94	3.48	3	18	1.191
VCS3	0.76	6.3	27.9	1970	1.497	0.616	7.04	2.95	3.47	2	16	1.171
VCT1	3.37	6.2	30.4	455	1.533	0.554	5.41	9.25	5.10	2	61	1.132
VCT2	3.45	6.2	28.1	437	1.508	0.612	6.87	9.19	5.08	3	91	1.143
VCT3	3.50	6.1	27.7	435	1.523	0.625	7.21	9.25	5.09		54	1.175
VCT4x	3.51	6.3	28.8	430	1.509	0.591	6.35	9.38	5.12	3	42	
VCF1	15.8	5.7	27.8	120	1.896	0.629	7.12	28.7	7.44	2		1.062
CS1	0.69	6.7	31.4	2178	1.503	0.522	4.95	2.85	3.44	3	27	1.145

Table 1 (*continued*)

Experiment	Q	T_{water}	T_{wax}	Duration	Final volume	θ_s	St	Pe	Nu	t_s	t_{b1}	D
	(cm^3 s^{-1})	(°C)	(°C)	(s)	(l)			($\times 10^{-3}$)		(s)	(s)	
CS2	0.76	6.5	31.2	1974	1.500	0.530	5.03	3.05	3.52	3	20	1.134
CS3	0.77	6.3	30.3	1958	1.508	0.554	5.46	3.05	3.53	5	25	1.292
CF1	16.7	6.2	32.2	115	1.921	0.515	4.63	31.3	7.66	3		1.060
PSH1	0.70	9.2	39.8	2273	1.591	0.340	2.89	3.15	3.50	4	27	1.158
PSH2	0.77	8.7	37.3	1953	1.504	0.381	3.30	3.29	3.57	1	44	1.136
PSH3	0.79	8.6	38.8	1910	1.509	0.364	3.04	3.41	3.60	5	36	1.154
PFH1	17.5	8.7	40.7	97	1.698	0.341	2.77	35.5	7.84	16	78	1.041
PFH2	17.5	8.9	40.8	93	1.628	0.335	2.75	35.5	7.84	13		1.035
PFH3x	17.5	8.8	41.1	90	1.575	0.334	2.72	35.6	7.84	3	68	1.059
VHS1	0.78	8.6	47.6	1933	1.508	0.282	2.09	3.62	3.68	7	40	1.127
VHS2	0.83	8.5	46.7	1824	1.514	0.291	2.15	3.78	3.72	6	30	1.137
VHS3	0.76	8.5	48.2	1964	1.493	0.280	2.04	3.56	3.66	5	37	
VHT1	3.66	8.4	49.1	420	1.537	0.275	1.98	11.6	5.46	9	72	1.154
VHT2	3.51	8.6	48.7	456	1.601	0.274	2.01	11.2	5.39	5	84	1.176
VHT3	3.60	8.5	48.7	424	1.526	0.276	2.01	11.5	5.42	3	62	1.188

In all cases, $\rho_{water} = 997.1$ kg m^{-3}. t_s is the time at which crust was seen first.

the surface of the initial wax flow solidified incompletely, being divided into four (or sometimes three) plates separated by narrow bands or rifts of molten wax (Fig. 1c). As wax continued to be erupted the plates were carried aside, similar to the 'rifting' morphology described by Fink and Griffiths [7,8]. Breakouts from weak points on the margin and surface produced lobes that were broader and flatter than those seen at lower effusion rates (Fig. 1d). The flow morphology matured as surface flows cooled or diverged into streams with lower flow rates, leading to a more rugged flow outline. Thus, in Fig. 1d, the smooth lower part of the flow was formed early in the flow history, whereas the more rugged upper and right hand margins were fed from cooler streams of diverted wax.

At low θ_s and low effusion rate (e.g. PSH1), a narrow levee formed around the edge of the wax, while the wax surface above the vent remained molten (Fig. 1e). Breakouts through the flow margin and frequent overflows of wax from above the vent led to broad flat lobes (Fig. 1f). Comparing this with Fig. 1b shows that for a given effusion rate, a decrease in θ_s causes the flow surface to be smoother and the flow margin to be less rugged.

Finally, at high effusion rate and low θ_s (e.g. PR3) the marginal levees tended to be discontinuous (Fig. 1g) and breakouts produced broad flat lobes with occasional surface folds of large wavelength (Fig. 1h). In this experiment the effusion rate was sufficient to keep the vent region from crusting over and surface-fed flows contributed to the overall morphology of the model lava.

5. Analysis of the results

5.1. Spreading rate

Fig. 2 contrasts the spreading rate of one experiment with a very high effusion rate and minimal surface solidification (B4, Table 1) with the spreading rates in four experiments with low effusion rate and considerable surface solidification at various values of θ_s. In experiment B4, the mean radius was well-described by the theory for spreading of isoviscous liquid. This contrasts with the experiments at low flow rate, which grew with more ragged outlines and with mean radius proportional to $t^{3/8}$, as predicted by [16] for the regime controlled by crust strength and buoyancy (Eq. 12). The wax in these four experiments spread more slowly than if solidification had been absent.

The observation of viscosity-controlled spread-

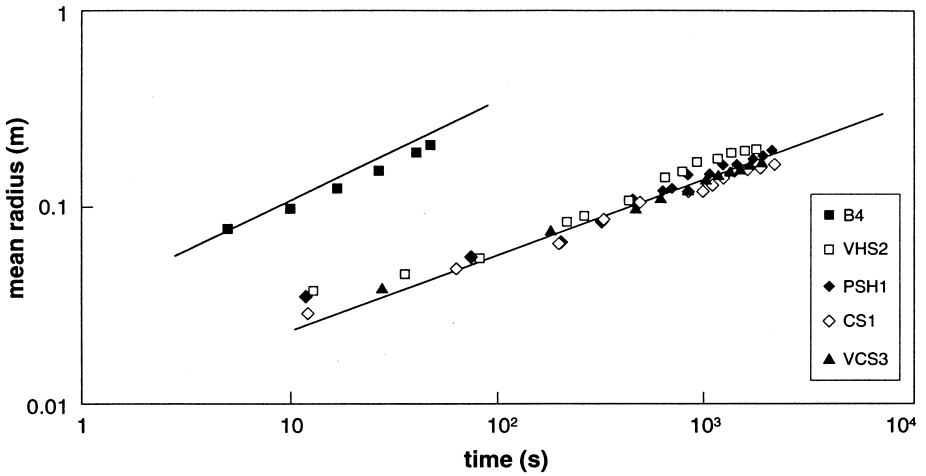

Fig. 2. Graph of mean radius versus time. The line passing close to the data for experiment B4 is the theoretical prediction for an isoviscous fluid, $R=0.6233(Q^3g\Delta\rho/\mu)^{1/8}t^{1/2}$ [17], with the initial properties of experiment B4. The remaining four experiments are described well by a line with a gradient of 3/8, which is the power law exponent for spreading limited by the strength of a thickening crust [16].

ing in B4 is important because it justifies the assumption made in Section 2 that viscosity, rather than inertia, controls the initial spreading of the wax. Viscosity-controlled spreading requires sufficiently low Q and high μ such that the transition time from inertia- to viscosity-control, $(Q\rho^2/g\Delta\rho\mu)^{1/2}$, is very short [17] or that the dimensionless group $S=(Q^3\rho^4g\Delta\rho/\mu^5)^{1/20}$ is of order 1 or less [23]. In experiment B4 these parameters have values of 1.8 s and 2.1, respectively, consistent with the good match between observation and viscous spreading theory. All other experiments had smaller values (due to lower Q and/or higher μ) and are therefore inferred to have started spreading under a viscosity–buoyancy force balance, as assumed in the model.

5.2. Timing of the first breakout

The time at which the flow margin first broke and let a stream of wax flow through the breached margin was recorded (Table 1). We refer to this time as the time of the first breakout, t_{b1}. The data show that for constant Q, t_{b1} decreases with increasing θ_s and that for constant θ_s, t_{b1} increases with increasing Q (Fig. 3). Because t_{b1} was much greater than the time at which crust first appeared, we can consider crust to have been growing throughout the flow's history and anticipate that t_{b1} scales with the time scale t_{crust} at which crust-dominated flow behaviour is established. We therefore compare t_{b1} with the predicted transition time scale t_c as a function of θ_s, St, Pe and Nu.

To characterise the surface heat flux, F, in each experiment, we adopt the argument of Fink and Griffiths [7] that the hot wax drives turbulent convection in the overlying water, such that:

$$F = 0.1\rho_a c_a\left(\frac{g\rho_a\alpha_a\kappa_a^2}{\mu_a}\right)^{1/3}(T_m-T_a)^{4/3} \qquad (20)$$

Subscript a refers to the property of the ambient water, α_a is the thermal expansivity of water. Values of α_a, c_a, κ_a, ρ_a and μ_a were taken from [12].

Given our values of T_m and T_a, St is very well-correlated with θ_s and Nu is very well-correlated with Pe (Table 1). Consequently, we need only compare t_{b1} with t_c as functions of θ_s and Pe. The data show that the normalised time of the first breakout t_{b1}/t_c decreases with θ_s and Pe (Fig. 4). Because $t_{b1}/t_c=(t_{b1}/t_{crust})/s^2$, these trends require that, if t_{b1}/t_{crust} is a constant, the value of s increases as both θ_s and Pe increase. A large value of s indicates a thicker crust is achieved in a given time, all else being equal (Eq. 6). From

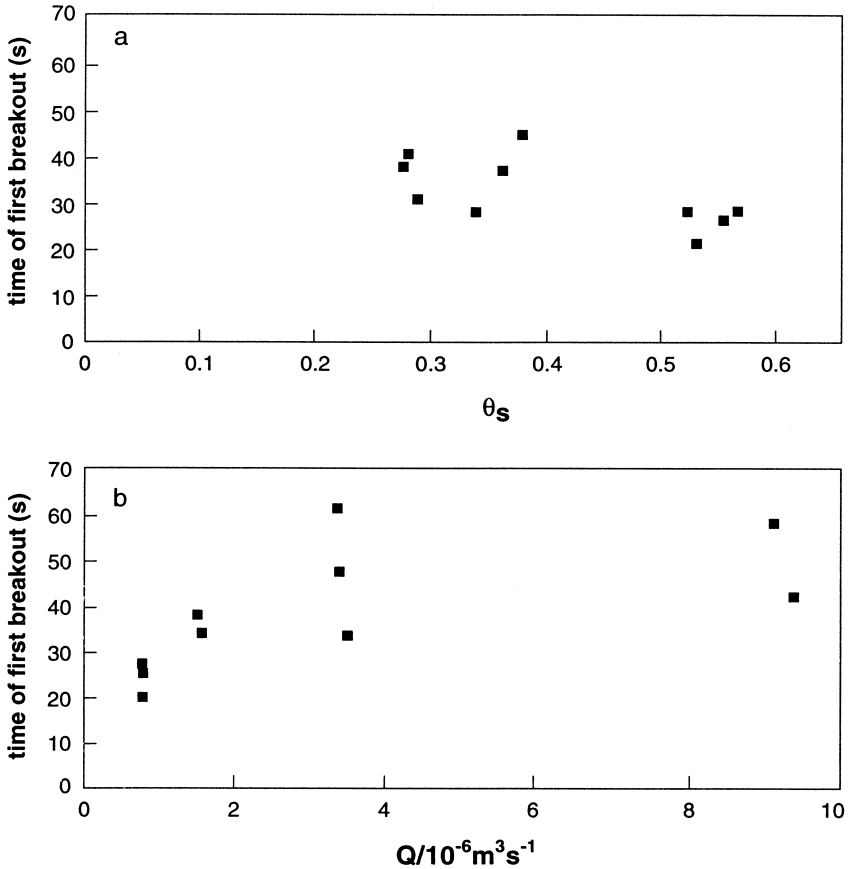

Fig. 3. The time of the first breakout is a function of (a) θ_s at an effusion rate of 7.6×10^{-7} m^3 s^{-1} and (b) effusion rate at $\theta_s = 0.55$.

Eq. 13, the larger the value of θ_s, the smaller the temperature drop required to reach the solidification temperature, so the solidification isotherm moves in to the flow faster than for small θ_s. In other words, large θ_s is expected to lead to large s, as inferred from Fig. 4a. In Fig. 4b, the negative trends between t_{b1}/t_c and Pe at constant θ_s can be compared with the forced correlation due to Q appearing in the variables plotted on both axes. This effect would give a slope of $-4/3$, which is somewhat steeper than shown by the data for given θ_s, so there is a real effect of Pe on breakout time, as already suggested by the correlation between t_{b1} and Q in Fig. 3b. This is most likely due to the enhanced advection of cool surface material to the flow front at high Pe. It is concluded that the first breakout occurred after the time scale t_c, which is a function of the parameters θ_s and Pe (and by inference St and Nu) that influence the rate of crust thickening at the flow front.

5.3. Estimation of crust strength

The normalising values of t_c in Fig. 4 used $\sigma = 40$ Pa, estimated from the scale height of flows governed by a balance between buoyancy and crust strength [16]. A different estimate can be made by equating t_{b1} to t_{crust} and rearranging to obtain

$$\sigma = \left(\frac{\mu g \Delta\rho Q}{t_{b1} s^2 \kappa}\right)^{1/2} \quad (21)$$

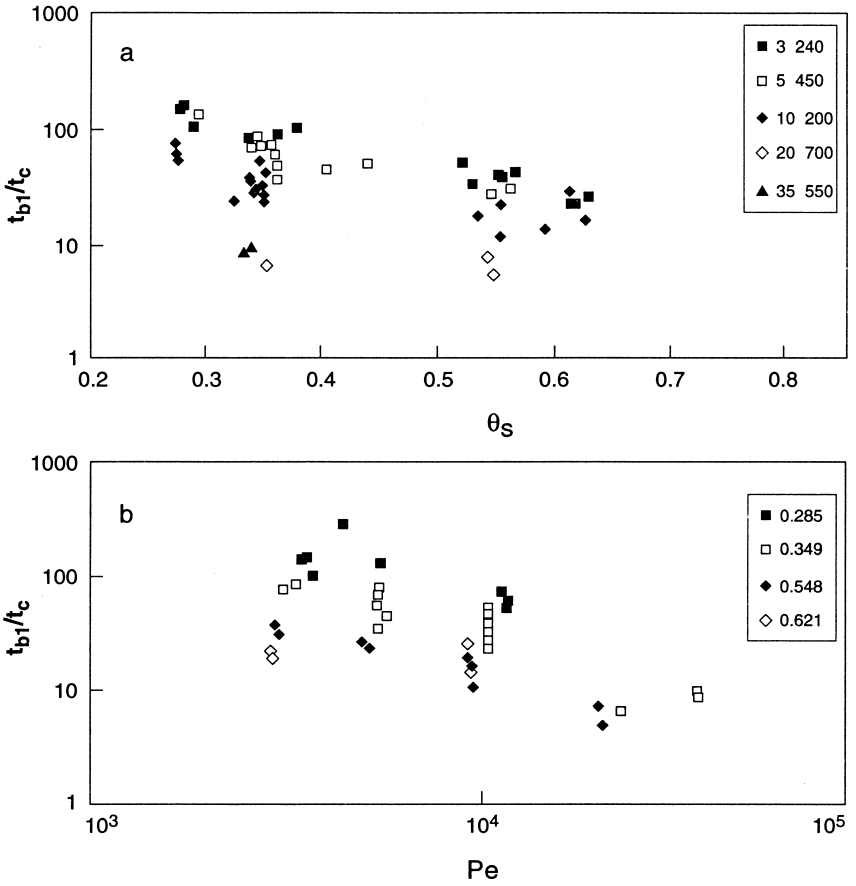

Fig. 4. (a) Normalised time of first breakout, t_{b1}/t_c, versus θ_s for five values of *Pe*. (b) t_{b1}/t_c versus *Pe* for four values of θ_s. Calculations assume $\sigma = 40$ Pa.

In the limit $Pe = 0$, s can be estimated using a model of conductive cooling of a wax layer whose surface is held at $T_a < T_{solid} < T_m$ ([21], Eq. 25):

$$s = \left(\frac{2\theta_s}{(1-\theta_s)\mathrm{St}}\right)^{1/2} - \frac{1}{\mathrm{St}\sqrt{3}} + \left(\frac{1-\theta_s}{8\theta_s \mathrm{St}^3}\right)^{1/2}\left(\frac{1}{3} - \frac{\theta_s^2}{2(1-\theta_s)^2} - \frac{\theta_s}{1-\theta_s}\right) \quad (22)$$

This equation gives values of s which increase from 0.3 to 0.6 as θ_s increases from 0.27 to 0.63. Calculating σ from Eqs. 21 and 22, plotting the result against *Pe* (Fig. 5) and extrapolating the trend to $Pe = 0$ implies a value for σ of between 10 and 15 Pa.

5.4. Long-term evolution of the flow fields

Most of our experimental flows evolved past the first breakout to construct a compound flow. We counted the number of times that a new flow unit extended beyond the flow margin. No distinction was made between flow units formed by breakouts around the crusted margin, leaks of wax from below the flow margin, or wax reaching the flow margin from boccas in the surface crust. The results for experiments with $Q \approx 8 \times 10^{-7}$ m^3 s^{-1} ($Pe \approx 3\ 240$) are shown in Fig. 6 and reveal that flows with higher values of θ_s produced more

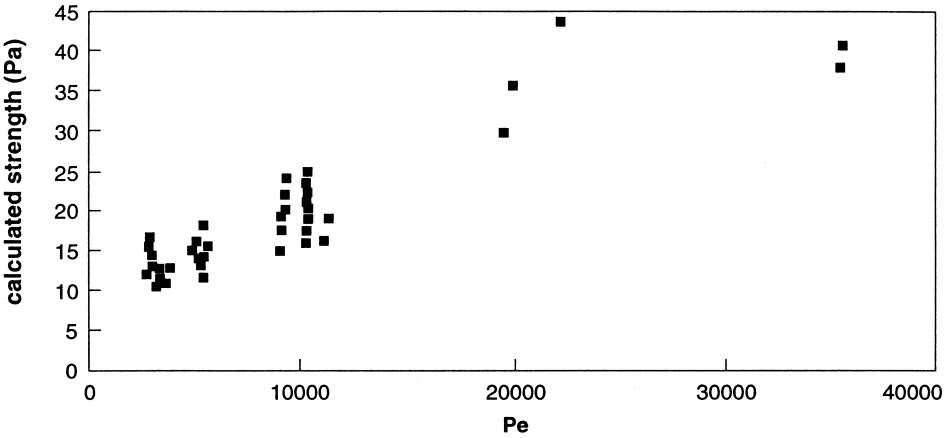

Fig. 5. Calculated crust strength, derived using Eqs. 21 and 22, plotted against *Pe*.

marginal flow lobes than experiments with lower θ_s. For $\theta_s = 0.62$ the number of marginal lobes increased almost linearly with time at a rate of $1/t_{crust}$ (hence the slope of 1 on Fig. 6) due to the successive production of flow lobes on a time scale of t_{crust}. In experiments with lower θ_s, the rate at which new lobes were added to the margin eventually diminished, most likely because surface breakouts solidified before reaching the flow margin. On the other hand, the frequency of breakouts exceeded $1/t_{crust}$ whenever a given lobe branched into two lobes, each necessarily with a flow rate less than Q, such that each minor lobe reached its breakout condition in a time less than t_{crust} defined by the total flow rate.

5.5. The fractal dimension of the flow margin

Bruno et al. [24,25] showed that the margins of basaltic lava flows are fractal, with shapes that can be quantified by a parameter called the fractal dimension (D). They used the 'structured-walk' method, entailing rods of various lengths being 'walked' along the flow margin. For each rod

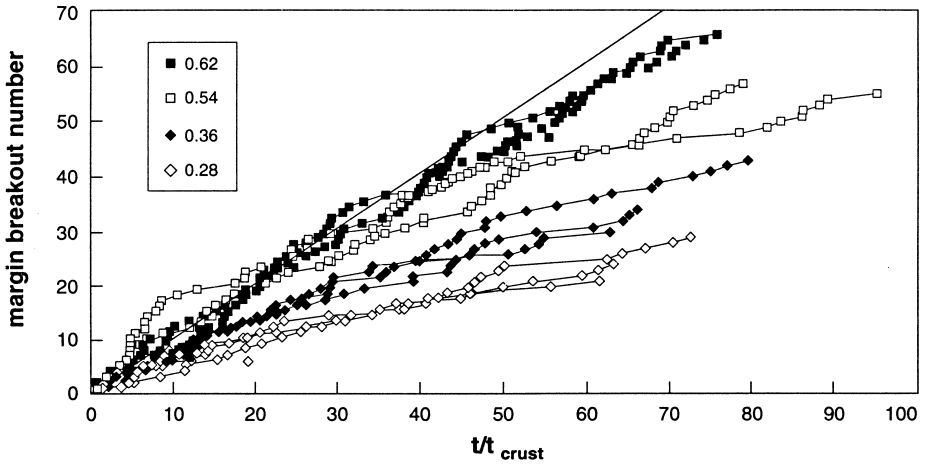

Fig. 6. The number of marginal flow lobes in experiments of given θ_s versus time normalised to t_{crust} calculated with s given by Eq. 22 and $\sigma = 13$ Pa.

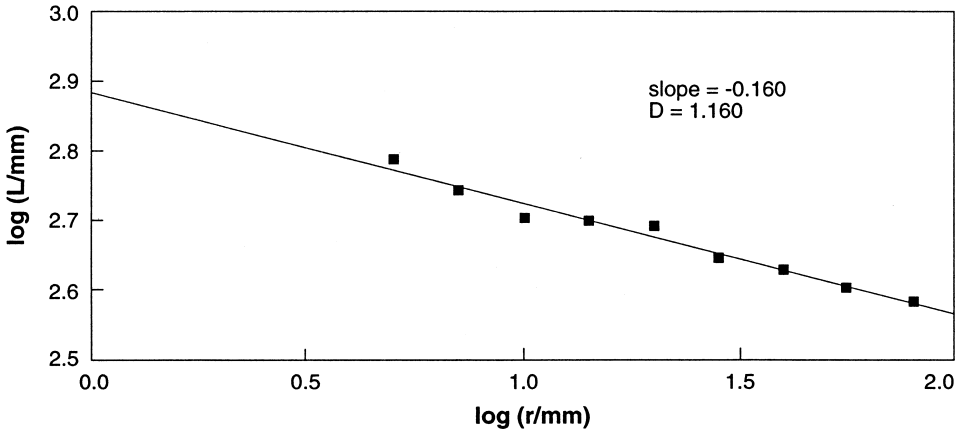

Fig. 7. The Richardson plot for the final flow outline of experiment PDR1.

length (r), the flow margin length (L) is determined according to the number (N) of rod lengths needed to approximate the margin (i.e. $L = Nr$). A linear trend with slope < 0 on a log(L) versus log(r) plot (a 'Richardson plot') indicates fractal behaviour, and D is simply $1-m$, where m is the slope of the linear least squares fit to the data. The D value is a measure of the area-filling character of the margin, the more rugged the margin, the greater its fractal dimension. Bruno et al. [25] found that aa lavas had $D = 1.05$ to 1.09 whereas pahoehoe flows had $D = 1.13$ to 1.23. Using an alternative technique ('box-counting') Gaonac'h et al. [26] found the perimeters of basaltic lava flow fields had $1.12 \leq D \leq 1.42$, although they combined flows from individual eruptions or entire volcanoes.

To shed light on the physical origins of the fractal characteristics of flow margins we used the structured-walk method to measure D values of the wax flows (Table 1 and Fig. 7). Fig. 8a shows D as a function of time normalised to t_c for experiments with $\theta_s = 0.35$. The data extend to a normalised time of about 10^2 and show an increase in D value with time. Plotting the D value obtained at the end of each experiment (Fig. 8b) shows D increasing with time until reaching a 'steady state' after $t/t_c \sim 10$. These results indicate that a growing wax flow field matures over time to reach a constant D, with no suggestion that θ_s determines the final 'steady state' value. The mean and standard deviation of the 35 data at $t/t_c > 10$ in Fig. 8b is 1.145 ± 0.037.

6. Application to lavas

The wax experiments and the theory that describes them indicate that, given sufficient time, any lava spreading over a flat surface will eventually attain the condition where the strength of the lava crust limits the spread of the lava, causing breakouts to form. In this section we interpret the morphologies of basaltic flows and silicic domes in terms of the parameters controlling the timing of breakouts.

Lava flow eruptions that continue for a time less than the breakout time t_{crust} will form a roughly circular dome, whereas those that last much longer than t_{crust} will undergo several breakouts and form a rock mass composed of several lobes, pillows or toes. Walker [1] made the point that compound lava flows are the typical result of slow effusion of low viscosity magma whereas simple lava flows result from higher effusion rates and from slow effusion of high viscosity magma. This is explained by our experimental results: lavas with many flow units form when the breakout time scale is much shorter than the duration of the eruption. Because $t_{crust} \propto$ viscosity $\times$ effusion rate, conditions for compound flows are favoured by small viscosity or small effusion rate, as postu-

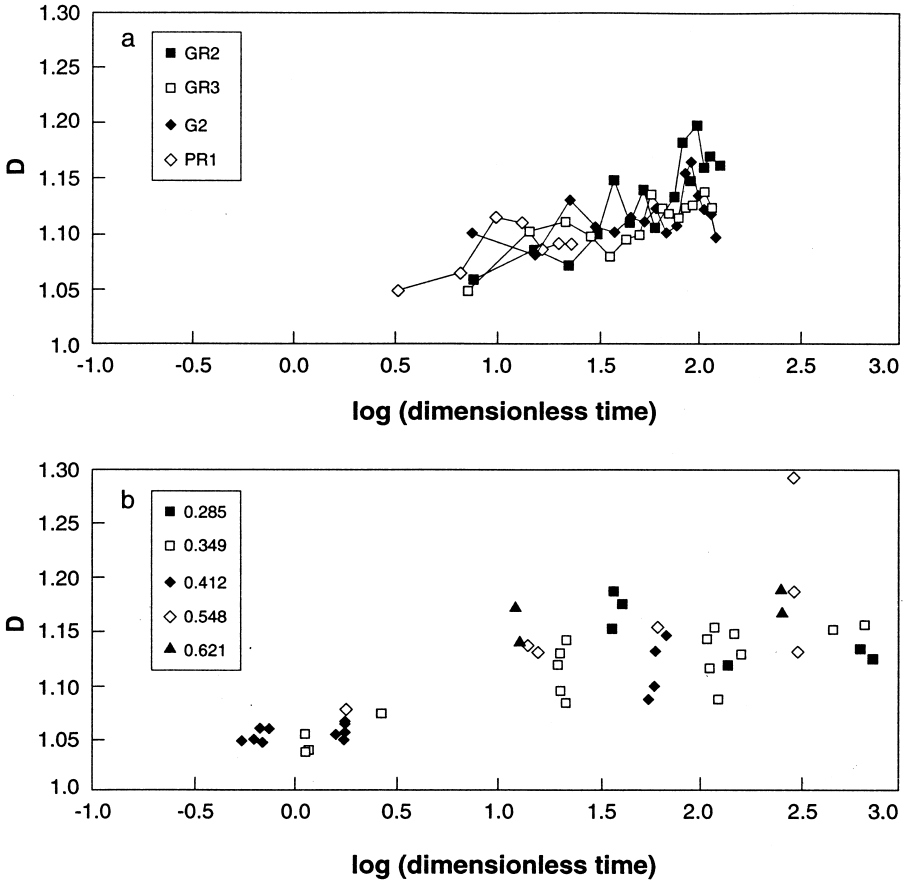

Fig. 8. Plots of D versus dimensionless time $t\sigma^2\kappa/g\Delta\rho\mu Q$ at (a) 1 min intervals in four experiments with $\theta_s = 0.35$ and (b) the end of experiments with $\theta_s \approx 0.285$, 0.349, 0.412, 0.548 and 0.621. Calculations assume $\sigma = 13$ Pa.

lated by Walker [1], but the duration of the eruption must also be considered. Furthermore, the criterion that a compound lava flow forms when the eruption continues to a time $t > t_{crust}$ can be expressed as:

$$\mu < \left(\frac{\sigma^2 s^2 \kappa}{g\Delta\rho}\right)\left(\frac{V}{Q^2}\right) \quad (23)$$

The reverse of this inequality defines the conditions for simple lava flows.

Data on the morphology, viscosity [27,28], volume and effusion rate of lavas erupted onto fairly flat ground from localised vents are collated in Table 2 and plotted on Fig. 9. Simple domes occupy the top left part of Fig. 9, separated by a band of unit slope from compound lavas occupying the bottom right. This result is anticipated by Eq. 23 for the case of constant σ and implies that the primary controls on flow development are the viscosity of the erupted magma and the ratio V/Q^2. Data for small lava lobes at the point they burst and fed another lobe plot on or close to the boundary between the fields of compound and simple flows, as expected. Uncertainties in μ, V and Q, and unavoidable departures from the assumptions of constant Q, perfectly horizontal ground and a point source vent make it unsurprising that the boundary between compound and simple flows on this diagram is a narrow band rather than a precise line. The position of the transition band implies that compound lavas are

Table 2
Lava flow data

Volcano and data source	Eruption	Volume (10^6 m^3)	Effusion rate (m^{3}s^{-1})	Viscosity (Pa s)	Composition	Type
Galunggung [34]	1918	8.5	7.6	1.0×10^7	andesite	simple dome
Tarumai [35]	1909	20	>116	10^7	andesite	simple dome
Barcena [36,37]	1952-3 lava	23.5	8.0	2.4×10^4	trachyte	simple flow
Soufriere, St. Vincent [22,38]	1979 dome	47.3	3.7	10^7	andesite	simple dome
Mt. St. Helens [39,40]	June 1980	4.7	8	3×10^{10}	dacite	simple dome
Mt. St. Helens [39,40]	August 1980	0.7	6.5	3×10^{10}	dacite	simple dome
Mt. St. Helens [39,40]	October 1980	1.5	35	10^{10}	andesite	simple dome
Parícutin [41,42]	Taqui flow 1944	64	3.5	10^3	bas. andesite	compound flow
Parícutin [41,42]	Quitzocho I 1943	7	13.5	10^3	bas. andesite	simple flow
Parícutin [41,42]	July–October 1948	14	2.3	1.1×10^4	andesite	simple flow
Piton de la Fournaise [43,44]	28/12/85–8/2/86	7	2	44	basalt	compound flow
Piton de la Fournaise [43,44]	10/6/87–29/6/87	1.5	0.9	44	basalt	compound flow
Etna [45,46]	June–September 1763	28	4	170	basalt	compound lava
Wudalianchi [47,48]	1719–1721	1000	10	100	phonotephrite	compound flow
Kilauea [2]	23 January 1988 lobe	0.0134	0.65	32	basalt	single sheet
Etna [49,50]	1975	0.5 m^3	5×10^{-4}	10^4	hawaiite	single toe
Etna [49,50]	1975	5 m^3	2×10^{-3}	10^4	hawaiite	single tongue
Kilauea	unpublished video	0.1 m^3	8.3×10^{-4}	10^2	basalt	single toe

formed when $\mu < 0.002V/Q^2$ and hence $(\sigma^2 s^2 \kappa / g\Delta\rho) \approx 2\times10^{-3}$ kg m^2 s^{-3}. Substituting representative values $s\kappa^{1/2} = 1.3\times10^{-3}$ m s$^{-1/2}$ [2], $g = 9.81$ m s^{-2} and $\Delta\rho = 2.6\times10^3$ kg m^{-3} gives $\sigma \sim 10^4$ Pa. Although all of the plotted points are consistent with this value, it is constrained only by information from basaltic to intermediate compositions.

The experiments described in Section 4 showed that once a compound morphology becomes established, the flow from the vent becomes distributed to several different regions. The size and lifetime of each breakout is then determined by the local supply rate, rather than the eruption rate at the vent, and by the local viscosity of the interior magma, which may be higher than that at the vent because of cooling or degassing. As the local

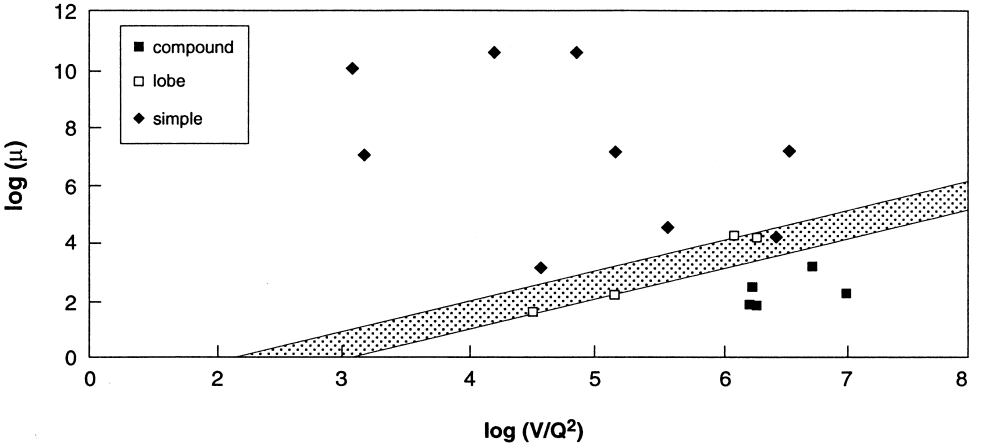

Fig. 9. Data for lava flows in Table 2 coded according to flow morphology. The band separating compound and simple flows covers a range of one order of magnitude in μ and V/Q^2.

flow rate is reduced, so the size of the breakouts decreases and their frequency increases. A large eruption rate can, if sustained for sufficient time, produce a mature compound flow with morphological elements reflecting low flow rates. This may explain why voluminous flood basalts often show compound morphology with small pahoehoe toes and lobes [1,29–31]. While this morphology has been taken as evidence of low eruption rates [29], our results indicate that it is actually the integrated effect of viscosity, eruption rate and time (or erupted volume, because $V = Qt$) that is critical. Flood basalts can show compound morphology at least partly because of large volume, and hence large V/Q^2, and not necessarily because of low Q. In particular, for basalts with $\mu \sim 10^2$–10^3 Pa s erupted from a point source a compound morphology is predicted to be present as long as $V/Q^2 > 10^5$ m^{-3} s^2 (Fig. 9). Likewise, for picrites and komatiites ($\mu < 10$ Pa s), the condition $V/Q^2 > 10^3$ m^{-3} s^2 will be sufficient to generate compound flows such as those described in [32, 33].

7. Conclusions

Experiments in which molten PEG wax is extruded from a point source under cold water are analogues of compound lava flows. The experiments produced breakouts on a time scale that is proportional to the product of lava viscosity and effusion rate divided by the strength of the lava crust squared (Eq. 11). The number of breakouts and the fractal dimension of the flow margin increased with time normalised by breakout time scale. When more than one breakout is active, the local flow rate for each breakout is less than the total eruption rate at the vent. This increases the rate at which more breakouts occur and the flow field matures into a complex collection of channels, lobes and pahoehoe toes. Central-vent eruptions of compound and simple flows on horizontal ground occupy separate fields on a plot of magma viscosity versus volume/(effusion rate squared). Compound lavas are formed when $\mu < 0.002 V/Q^2$. Thus, morphologies associated with low flow rates can develop whatever the total effusion rate if sufficient time (volume erupted) is available.

Acknowledgements

Experiments were funded by the Open University Research Development Funding Subcommittee. S.B. gratefully acknowledges Scion Natural Science Association for supporting travel to the Geology Department, Arizona State University, where parts of the paper were written, and thanks Jon Fink and colleagues for their hospitality. We thank R.W. Griffiths, J.H. Fink and D.T. Lescinsky for helpful comments, and S. Rowland and L. Keszthelyi for useful reviews.*[FA]*

References

[1] G.P.L. Walker, Compound and simple lava flows and flood basalts, Bull. Volcanol. 35 (1972) 579–590.
[2] K. Hon, J. Kauahikaua, R. Denlinger, K. Mackay, Emplacement and inflation of pahoehoe sheet flows: observations and measurements of active lava flows on Kilauea Volcano, Hawaii, Geol. Soc. Am. Bull. 106 (1994) 351–370.
[3] D.W. Peterson, R.T. Holcomb, R.I. Tilling, R.L. Christiansen, Development of lava tubes in the light of observations at Mauna Ulu, Kilauea Volcano, Hawaii, Bull. Volcanol. 56 (1994) 343–360.
[4] C.R.J. Kilburn, Lava crusts, aa flow lengthening and the pahoehoe-aa transition, in: C.R.J. Kilburn, G. Luongo (Eds.), Active Lavas: Monitoring and Modelling, UCL Press, London, 1993, pp. 263–279.
[5] C.R.J. Kilburn, H. Pinkerton, L. Wilson, Forecasting the behaviour of lava flows, in: W.J. McGuire, C.R.J. Kilburn, J.B. Murray (Eds.), Monitoring Active Volcanoes, UCL Press, London, 1995, pp. 346–368.
[6] M.A. Hallworth, H.E. Huppert, R.S.J. Sparks, A laboratory simulation of basaltic lava flows, Mod. Geol. 11 (1986) 93–107.
[7] J.H. Fink, R.W. Griffiths, Radial spreading of viscous-gravity currents with solidifying crust, J. Fluid Mech. 221 (1990) 485–509.
[8] J.H. Fink, R.W. Griffiths, A laboratory analog study of the surface morphology of lava flows from point and line sources, J. Volcanol. Geotherm. Res. 54 (1992) 19–32.
[9] J.A. Whitehead, P. Keleman, Fluid and thermal dissolution instabilities in magmatic systems, in: M.P. Ryan (Ed.), Magmatic Systems, Academic Press, 1994, pp. 355–379.

[10] T.K.P. Gregg, J.H. Fink, Quantification of submarine lava-flow morphology through analog experiments, Geology 23 (1995) 73–76.
[11] J.H. Fink, N.T. Bridges, Effects of eruption history and cooling rate on lava dome growth, Bull. Volcanol. 57 (1995) 229–239.
[12] R.W. Griffiths, J.H. Fink, Solidifying Bingham extrusions: a model for the growth of silicic lava domes, J. Fluid Mech. 347 (1997) 13–36.
[13] J.H. Fink, R.W. Griffiths, Morphology, eruption rates, and rheology of lava domes: insights from laboratory models, J. Geophys. Res. 103 (1998) 527–545.
[14] R.W. Griffiths, J.H. Fink, Solidification and morphology of submarine lavas: a dependence on extrusion rate, J. Geophys. Res. 97 (1992) 19729–19737.
[15] R.W. Griffiths, J.H. Fink, The morphology of lava flows in planetary environments: predictions from analog experiments, J. Geophys. Res. 97 (1992) 19739–19748.
[16] R.W. Griffiths, J.H. Fink, Effects of surface cooling on the spreading of lava flows and domes, J. Fluid Mech. 252 (1993) 667–702.
[17] H.E. Huppert, The propagation of two-dimensional and axisymmetric viscous gravity currents over a rigid horizontal surface, J. Fluid Mech. 121 (1982) 43–58.
[18] H.S. Carslaw, J.C. Jaeger, Conduction of Heat in Solids, 2nd edn., Oxford University Press, 1959.
[19] T.K.P. Gregg, D.J. Fornari, Long submarine lava flows: observations and results from numerical modeling, J. Geophys. Res. 103 (1998) 27517–27531.
[20] J.G. Moore, Mechanism of formation of pillow lava, Am. Sci. 63 (1975) 269–277.
[21] C. Charach, P. Zoglin, Solidification in a finite, initially overheated slab, Int. J. Heat Mass Transf. 28 (1985) 2261–2268.
[22] M.V. Stasiuk, C. Jaupart, R.S.J. Sparks, Influence of cooling on lava-flow dynamics, Geology 21 (1993) 335–338.
[23] G.N. Ivey, S. Blake, Axisymmetric withdrawal and inflow in a density-stratified container, J. Fluid Mech. 161 (1985) 115–137.
[24] B.C. Bruno, G.J. Taylor, S.K. Rowland, P.G. Lucey, S. Self, Lava flows are fractals, Geophys. Res. Lett. 19 (1992) 305–308.
[25] B.C. Bruno, G.J. Taylor, S.K. Rowland, S.M. Baloga, Quantifying the effect of rheology on lava-flow margins using fractal geometry, Bull. Volcanol. 56 (1994) 193–206.
[26] H. Gaonac'h, S. Lovejoy, J. Stix, Scale invariance of basaltic lava flows and their fractal dimensions, Geophys. Res. Lett. 19 (1992) 785–788.
[27] H.R. Shaw, Viscosities of magmatic silicate liquids: an empirical method of prediction, Am. J. Sci. 272 (1972) 870–893.
[28] B.D. Marsh, On the crystallinity, probability of occurrence and rheology of lava and magma, Contrib. Miner. Petrol. 78 (1981) 85–98.
[29] S. Self, Th. Thordarson, L. Keszthelyi, G.P.L. Walker, K. Hon, M.T. Murphy, P. Long, S. Finnemore, A new model for the emplacement of Columbia River basalts as large, inflated pahoehoe lava flow fields, Geophys. Res. Lett. 23 (1996) 2689–2692.
[30] S. Self, Th. Thordarson, L. Keszthelyi, Emplacement of continental flood basalt lava flows, in: J.J. Mahoney, M. Coffin (Eds.), Large Igneous Provinces: Continental, Oceanic and Planetary Flood Volcanism, AGU Geophysical Monograph 100 (1997) 381–410.
[31] S. Self, L. Keszthelyi, Th. Thordarson, The importance of pahoehoe, Annu. Rev. Earth Planet. Sci. 26 (1998) 81–110.
[32] R.E.T. Hill, S.J. Barnes, M.J. Gole, S.E. Dowling, The volcanology of komatiites as deduced from field relationships in the Norseman-Wiluna greenstone belt, Western Australia, Lithos 34 (1995) 159–188.
[33] R. Cas, S. Self, S. Beresford, The behaviour of the fronts of komatiite lavas in medial to distal settings, Earth Planet. Sci. Lett. 172 (1999) 127–139.
[34] M.-C. Gerbe, A. Gourgaud, O. Sigmarsson, R.S. Harmon, J.-L. Joron, A. Provost, Mineralogical and geochemical evolution of the 1982–1983 Galunggung eruption (Indonesia), Bull. Volcanol. 54 (1992) 284–298.
[35] Y. Katsui, H. Yamagishi, T. Soya, Y. Watanabe, M. Nakagawa, Cenozoic volcanism in southwestern Hokkaido, in: H. Kato, H. Noro (Eds.), 29th IGC Field Trip Guidebook, Vol. 4: Volcanoes and Geothermal Fields of Japan, Geological Survey of Japan, Tsukuba, Japan, 1992, pp. 1–28.
[36] A.F. Richards, Geology of the Islas Revillagigedo, Mexico 1. Birth and development of Volcán Bárcena, Isla San Benedicto, Bull. Volcanol. 22 (1959) 73–124.
[37] A.F. Richards, Geology of the Islas Revillagigedo, Mexico 2. Geology and petrography of Isla San Benedicto, Proc. Calif. Acad. Sci. Fourth Ser. 33 (1966) 361–414.
[38] H.E. Huppert, J.B. Shepherd, H. Sigurdsson, R.S.J. Sparks, On lava dome growth, with application to the 1979 lava extrusion of the Soufriere of St. Vincent, J. Volcanol. Geotherm. Res. 14 (1982) 199–222.
[39] J.G. Moore, P.W. Lipman, D.A. Swanson, T.R. Alpha, Growth of lava domes in the crater, June 1980–January 1981, U.S. Geol. Surv. Prof. Pap. 1250 (1981) 541–547.
[40] M. Alidibirov, D.B. Dingwell, R.J. Stevenson, K.-U. Hess, S.L. Webb, J. Zinke, Physical properties of the 1980 Mount St. Helens cryptodome magma, Bull. Volcanol. 59 (1997) 103–111.
[41] J.F. Luhr, T. Simkin, Parícutin, the Volcano born in a Mexican Cornfield, Geoscience Press, Phoenix, AZ, 1993, p. 427.
[42] M.V. Stasiuk, C. Jaupart, R.S.J. Sparks, On the variations of flow-rate in nonexplosive lava eruptions, Earth Planet. Sci. Lett. 114 (1993) 505–516.
[43] Bulletin of Volcanic Eruptions, No. 27, Suppl. to Bull. Volcanol. 52 (1990) 7–9.
[44] F. Albarède, V. Tamagnan, Modelling the recent evolution of the Piton de la Fournaise volcano, Réunion Island, 1931–1986, J. Petrol. 29 (1988) 997–1030.
[45] F. Mulargia, S. Tinti, E. Boschi, A statistical analysis of

flank eruptions on Etna volcano, J. Volcanol. Geotherm. Res. 23 (1985) 263–272.
[46] N. Metrich, R. Clocchiati, Melt inclusion investigation of the volatile behaviour in historic alkali basaltic magmas of Etna, Bull. Volcanol. 51 (1989) 185–197.
[47] M. Feng, J.L. Whitford-Stark, The 1719–1721 eruptions of potassium-rich lavas at Wudalianchi, China, J. Volcanol. Geotherm. Res. 30 (1986) 131–148.
[48] R.O. Sack, D. Walker, I.S.E. Carmichael, Experimental petrology of alkalic lavas: constraints on cotectics of multiple saturation in natural basic liquids, Contrib. Miner. Petrol. 96 (1987) 1–23.
[49] H. Pinkerton, R.S.J. Sparks, The 1975 sub-terminal lavas, Mount Etna: a case history of the formation of a compound lava field, J. Volcanol. Geotherm. Res. 1 (1976) 167–182.
[50] H. Pinkerton, R.S.J. Sparks, Field measurements of the rheology of lava, Nature 276 (1978) 383–385.